ELSEVIER

Polymer 42 (2001) 7141–7151

polymer

www.elsevier.nl/locate/polymer

In situ study of structure development in poly(trimethylene terephthalate) fibers during stretching by simultaneous synchrotron small- and wide-angle X-ray scattering

J. Wu[a], J.M. Schultz[a,*], J.M. Samon[a], A.B. Pangelinan[b], H.H. Chuah[b]

[a]*Department of Chemical Engineering, University of Delaware, Newark, DE 19716, USA*
[b]*Westhollow Technology Center, Shell Chemical Company, Houston, TX 77251, USA*

Received 15 September 2000; received in revised form 27 November 2000; accepted 3 January 2001

Abstract

In this study, simultaneous synchrotron small-angle X-ray scattering (SAXS) and wide-angle X-ray diffraction (WAXD) on as-spun and on spun and subsequently drawn poly(trimethylene terephthalate) (PTT) fibers under cold and hot stretch-hold operations were performed. Crystallinity and orientation analyses were performed on WAXD patterns, while correlation function analysis was used to analyze SAXS patterns to determine the long period. For spun and drawn fibers, WAXD patterns suggested that unit cell dimensions, crystallinity and orientation were dependent on stretching temperature and strain. From orientation analysis, it was reasonable to infer that a rigid amorphous phase existed in the drawn fibers. From SAXS patterns, a defectively stacked lamellar structure was induced at 120°C. Further application of strain up to 100% at 120°C triggered a lamellar to fibrillar transition, as suggested by the formation of a pair of very weak narrow streaks perpendicular to the meridian in the WAXD pattern. These streaks imply a microfibrillar entity. For as-spun fibers, strain could only induce micro-crazes, whose planes are perpendicular to the fiber axis, but could not induce crystallization. At 120°C, WAXD patterns showed that a new transitional phase was formed, which could be transformed to the equilibrium structure with application of strain over 100%.

Keywords: Poly(trimethylene terephthalate); Fibers; Small- and wide-angle X-ray scattering

1. Introduction

Poly(trimethylene terephthalate) (PTT), also known as 3GT, belongs to the polyester family, among which both poly(ethylene terephthalate) (PET) and poly(butylene terephthalate) (PBT) are important members. PET and PBT have been studied thoroughly during the last decades. The crystal structure of PTT was determined by Desborough et al. [1] and Dandurand et al. [2]. According to Desborough [1], the unit cell of PTT is triclinic with $a = 4.6$ Å, $b = 6.2$ Å, $c = 18.3$ Å, $\alpha = 98°$, $\beta = 90°$ and $\gamma = 112°$. The space group is $P\bar{1}$. Each cell contains two monomers of one polymer chain. The molecular configuration consists of rigid planar terephthaloyl residues alternating with a more flexible trimethylene sequence. The $O–CH_2–CH_2–CH_2–O$ segment of the chain has a *trans–gauche–gauche–trans* conformation. The unit cell parameters reported by Dandurand [2] are very close to those from Desborough [1]. Crystal deformation of PTT fiber was studied by Jakeways et al. [3] who reported that PTT had an elastic unit cell, which responded immediately to the applied stress. Mechanical properties of PTT were studied by Ward et al. [4] and were compared to other polyester fibers. Except for these, there is little literature addressing the structure and morphology of PTT because the production of PTT was not industrialized. With the recent commercialization of PTT and its entrance to the fiber and thermoplastic application field, it has become useful to study the structure development of PTT fibers during processing. In this study, in situ simultaneous synchrotron small- and wide-angle X-ray scattering (SWAXS) measurements were carried out to investigate PTT fibers under cold and hot stretching. We are interested in not only the dependence of crystal structure and morphology on temperature and stress but also the relationship between morphological and crystal structure change.

2. Experimental

The PTT fibers were provided by Shell Chemical Company. They consisted of as-spun fibers (ASF) and

* Corresponding author. Tel.: +1-302-831-2543; fax: +1-302-831-1048.
E-mail address: schultz@che.udel.edu (J.M. Schultz).

0032-3861/01/$ - see front matter
PII: S0032-3861(01)00042-8

Table 1
Experimental condition for various fibers. (Strain usually ranges from 0 to 150%; +, scattering performed; −, scattering not performed)

T (°C)	UOF	OF, DR = 2 : 1	OF, DR = 3 : 1	OF, DR = 3.3 : 1
25	+	+	+	+
50	+	−	+	+
120	+	+	−	−

spun and subsequently oriented fibers (SOF) under draw ratios (DR) of 2:1, 3:1, 3.3:1. Synchrotron X-ray measurement was carried out at the Advanced Polymers Beamline (X27C) of the National Synchrotron Light Source, Brookhaven National Laboratory ($\lambda = 1.307$ Å, beam diameter = 370 μm). An Instron unit (Model 4222), modified to perform symmetric stretching, was used to apply strain to the above-listed fibers. A special heating rod was designed to heat the fiber without contact. The oriented and unoriented fibers were stretched to a certain strain and held for 2 min before the 2D WAXD and SAXS scattering patterns were recorded simultaneously by two Fuji™ HR-V imaging plates. The imaging plates were digitized by a Fuji™ BAS 2000 scanner with a resolution of 100 μm for both WAXD and SAXS patterns. Then the fibers were stretched to another strain level and the cycle repeated. Efforts were exerted to ensure that the fibers were vertical to the primary X-ray beam during the experiment. A central hole of 2.5 cm diameter was cut on each WAXD imaging plate to allow passage and registration of the SAXS signal. The typical collection time for WAXD patterns and SAXS patterns was 2 min. The recorded WAXD and SAXS patterns or their corresponding 1D-extracted profiles were subject to background and scattering volume corrections. The experimental conditions for these fibers are shown Table 1.

A double-multilayer (silicon/tungsten) monochromator is used to monochromatize the beam. The wavelength of the monochromatized beam is 1.307 Å with an energy resolution of 1.1%, which gives rise to a relative error of 1.1% for the d-spacing measurement.

3. Data analysis

3.1. Overall crystallinity index from WAXD

The center on the WAXD pattern was first determined based on the symmetrical reflections before integration along the azimuthal direction from 0 to 360° for all diffraction angles (2θ) was carried out. The integrated value at a given diffraction angle was then normalized by the number of pixels contributing to the integration. The resultant profile was similar to a usual X-ray powder diffraction pattern (intensity vs diffraction angle (2θ)) and would be termed a powder curve. This curve was then deconvoluted into individual indexed peaks and amorphous halo using the Levenberg–Marquardt method [5]. The peak type was chosen to be Gaussian and the peak position of the amorphous halo was confined to an angular region 1°.

The overall crystallinity index is given by the following formula [6]:

$$\text{Crystallinity index} = \frac{A_c}{A_c + A_a} \tag{1}$$

where A_c and A_a are the sum of areas under the crystalline and amorphous peaks, respectively. A typical 2D WAXD pattern and its corresponding 1D powder curve are shown in Fig. 1. The deconvoluted constituent peaks are shown as well.

The errors originating from the peak deconvolution are obtained by calculating the percentage of the residuals from the peak deconvolution. In addition to this error, there will

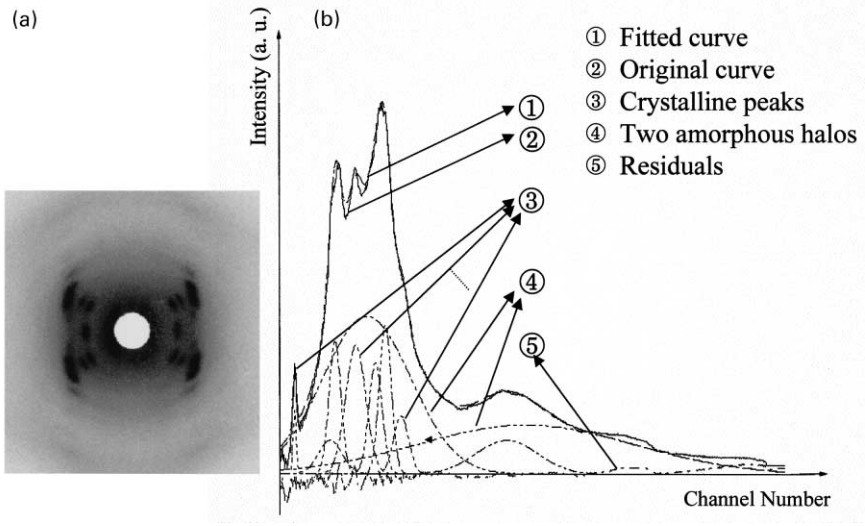

Fig. 1. Illustration of calculation of crystallinity from 2D WAXD pattern: (a) a Raster image of WAXD pattern; (b) a portion of the corresponding 1D powder curve.

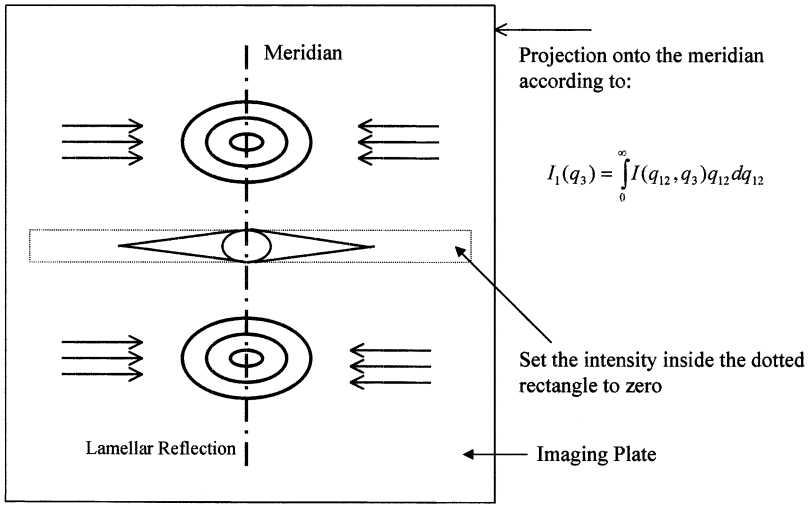

Fig. 2. Diagram for correlation function analysis.

be systematic errors deriving from the imprecision of a purely Gaussian fit. It is likely that these systematic errors will be roughly equivalent in all patterns.

3.2. Orientation of the crystallites from WAXD

The azimuthal profile of the 010 reflection was extracted and used to calculate the Hermans orientation factor f using the method suggested by Wilchinsky [7–11]. The orientation factor f derives from the second moment of the orientation of the chains with respect to the fiber axis. It should be noted that the method suggested by Stein [12] for determination of the orientation of crystallites having an orthorhombic unit cell is not applicable for this case because the unit cell of PTT is triclinic. The orientation factor f is given by:

$$f = \frac{3\langle\cos^2 \phi_{c,z}\rangle - 1}{2} \tag{2}$$

where $\langle\cos^2 \phi_{c,z}\rangle$ is the averaged value of the square of the cosine of the angle ϕ between the reference direction in the sample (fiber axis) and the polymer chain. The values of f can range from -0.5, when the chains are perpendicular to the fiber axis, to 1.0, when the chains are parallel to the fiber axis. When f equals zero, there is random orientation of chains with respect to the fiber axis in the sample [10].

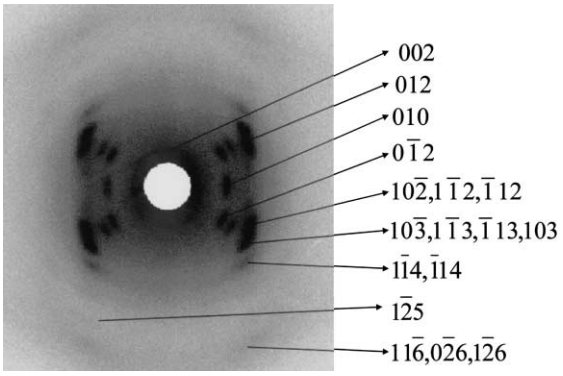

Fig. 3. Raster image of a 2D WAXD pattern with indexed reflections.

Assuming cylindrical symmetry in fiber, it is easy to show that $\langle\cos^2 \phi_{c,z}\rangle$ is given by the following equation:

$$\langle\cos^2 \phi_{c,z}\rangle = \frac{1 - g^2 - 2\langle\cos^2 \phi_{hkl,z}\rangle}{1 - 3g^2} \tag{3}$$

where g is the direction cosine of the norm of the (hkl) crystallographic plane with respect to the polymer chain and $\langle\cos^2 \phi_{hkl,z}\rangle$ is the averaged value of the square of the cosine of the angle ϕ between the fiber axis and the norm of the (hkl) crystallographic plane. For the 010 reflection, $g = 0$.

Assuming simple cylindrical symmetry of each planar normal about the fiber axis,

$$\langle\cos^2 \phi_{hkl,z}\rangle = \frac{\int_0^{\pi/2} I(\phi) \cos^2 \phi \sin \phi \, d\phi}{\int_0^{\pi/2} I(\phi) \sin \phi \, d\phi} \tag{4}$$

where $I(\phi)$ is the intensity diffracted from the (hkl) plane.

3.3. SAXS analysis to calculate the dimensions of lamellar morphology

The 2D SAXS pattern bearing a two-lobe feature suggests the existence of a stacked lamellar structure, i.e. stacks of alternating crystalline and non-crystalline regions. During our experiment, SAXS patterns having this feature were observed under certain conditions.

Table 2
Crystallinity dependence on draw ratio

DR	Crystallinity index (%)	Error (%)
2:1	6.1	± 0.08
3:1	26.0	± 0.08
3.3:1	23.4	± 0.15

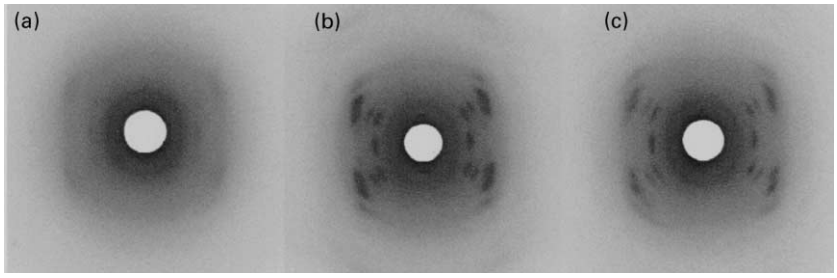

Fig. 4. 2D raster image of WAXD pattern illustrating processed draw ratio effect: (a) draw ratio = 2:1; (b) draw ratio = 3:1; (c) draw ratio = 3.3:1.

The correlation function ($\gamma(r)$) analysis method [13] was adopted to quantitatively analyze the lamellar structure. For this analysis, a projection operation was first applied to obtain the integrated intensity on the meridian ($I_1(q_3)$) using the following formalism:

$$I_1(q_3) = \int_0^\infty I(q_{12}, q_3) q_{12}\, \mathrm{d}q_{12} \tag{5}$$

where $q = 4\pi \sin\theta/\lambda$ is the scattering vector. The subscript 3 represents the meridianal direction and the subscript 12 represents equatorial directions. In order to obtain scattering intensity profiles solely from the lamellar structure, the intensity in a rectangular region, whose height just covers the beam stop, was set to zero to exclude scattering from the beam stop and microvoids before the projection operation was performed. This operation is illustrated in Fig. 2.

After obtaining $I_1(q_3)$, a 1D Fourier transformation was then applied to it to obtain the correlation function:

$$\gamma(x) = \frac{\int_0^\infty I_1(q_3) \cos(q_3 x)\, \mathrm{d}q_3}{\int_0^\infty I_1(q_3)\, \mathrm{d}q_3} \tag{6}$$

Using the method proposed by Strobl and Schneider [13] and assuming a lamellar two-phase morphology, the long period L and the lamellar and amorphous layer thicknesses can be evaluated.

4. Results

4.1. Spun and subsequently drawn fibers

The diffraction peaks in the WAXD patterns were indexed according to the parameters given by Desborough [1]. A 2D WAXD pattern (raster image) with indexed reflections is shown in Fig. 3. Along with indexing the reflections, the d-spacings of 002 and 010 were extracted.

4.1.1. The effect of draw ratio on crystallinity from WAXD

The qualitative effect of draw ratio on fiber crystallinity at 25°C is illustrated in Fig. 4. Comparing Fig. 4(a) with (b), it is observed that crystallinity increased when the draw ratio was increased from 2:1 to 3:1. However, when the draw ratio was further increased to 3.3:1, as shown in Fig. 4(c), the crystallinity began to decrease, as seen by comparing Fig. 4(b) with (c). In order to confirm this observation, a crystallinity calculation was carried out following the method described above.

The calculated results are shown as Table 2. The second column of Table 2 shows the calculated crystallinity index, while the third column shows the absolute error arising from the peak deconvolution process, which is estimated by the percentage of the residuals from the peak deconvolution. Our method for evaluating crystallinity of oriented sample has its systematic errors. The most correct one to access the crystallinity of an oriented system can be obtained by the full reciprocal space method of Ruland and Dewaelheyns [14]. The systematic error of our method may come from failing to include the missing meridianal reflection contribution or from accounting for intracrystalline defects within the amorphous phase. If the contribution of the missing meridianal peaks after the spherical averaging correction is small, the above-described method may approximate the true crystallinity. Furthermore, we believe the difference between the calculated and the true crystallinity, i.e. the systematic error, will be consistent between the images

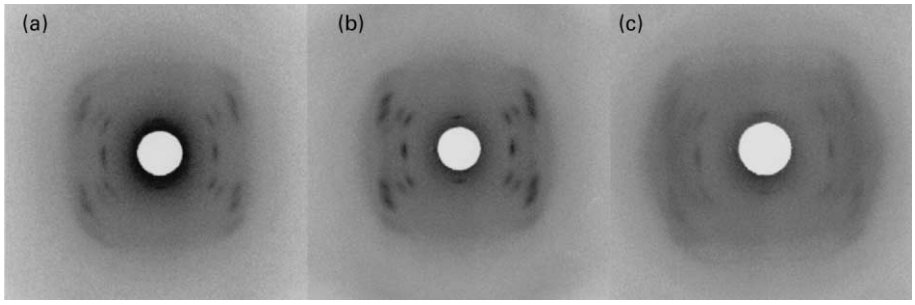

Fig. 5. Strain effect illustrated by 2D WAXD pattern from fiber of processed draw ratio 3.3:1 at 25°C: (a) strain = 0%, (b) strain = 40%, (c) strain = 100%.

and the result can be used for comparison purposes. It is hard to estimate this systematic error. Assuming it is consistent between images, the errors listed in Table 2 are the additional error arising from the peak deconvolution process, which is very small. It is also to be noted that our method has its limitations. When the crystallites are either small or very defective or when the crystallinity is very low, the resulting peak is broad and serious overlapping makes it impossible to obtain a good deconvolution. This is why we do not report crystallinity values of fibers of draw ratio of 2:1 at 25°C and that of fibers at 120°C.

It is known that the effect of drawing can be to annihilate small crystals and to induce secondary crystallization [15]. The results from Table 2 suggest that the crystallization effect dominates when draw ratios are between 2:1 and 3:1. The annihilation effect begins to take over when the draw ratio is increased to 3.3:1.

4.1.2. The effect of in situ strain at 25°C on crystallinity and cell dimension from WAXD

Representative 2D WAXD patterns illustrating the effect of in situ strain are shown in Fig. 5, where fibers of processed draw ratio of 3.3:1 were stretched from 0 to 100% strain. Similar to the effect of draw ratio, the strain first induced crystallization, as shown in Fig. 5(a) and (b), followed by crystal destruction, as illustrated in Fig. 5(b) and (c). It must be mentioned that strain will be used throughout this paper to express the extent of stretching. The true stress value was hard to measure because it quickly decayed during the holding period of the stretch-hold operation. On the other hand, strain was easy to obtain and the degree of stretching was well represented by it.

The crystallinity development was calculated for all strains for the fibers of as-processed draw ratio of 3.3:1 and is shown in Fig. 6 where it was observed that crystallinity reaches its maximum near 30% strain and then begins

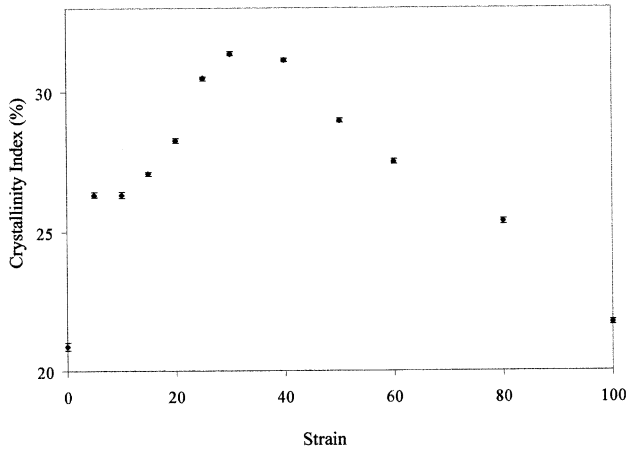

Fig. 6. Crystallinity versus strain curve for fiber of processed draw ratio of 3.3:1 at 25°C.

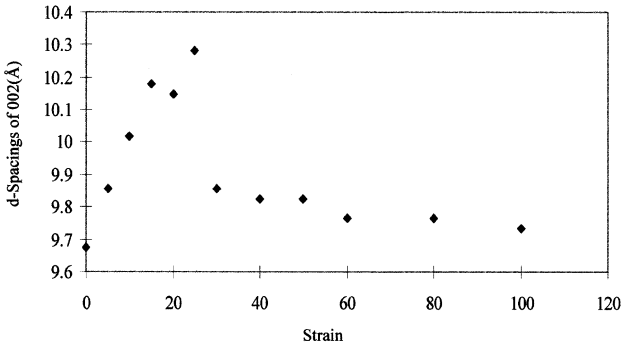

Fig. 7. The effect of strain on 002 *d*-spacing of fiber of processed draw ratio of 3.3:1 at 25°C.

to drop. The meaning of the error and its estimation method are the same as above.

It was reported [3,4] that the crystal lattice of PTT was fairly compliant because the authors observed the shift of certain reflections by applying stress. Our data confirmed this observation. The *d*-spacings of 002 reflections and 010 reflections of fibers processed to a 3.3:1 draw ratio were extracted and plotted against strain in Figs. 7 and 8, respectively. With the application of strain up to 25%, *d*-spacings of 002 increased, corresponding to elongation of the *c* axis of the cell, while the *d*-spacings of 010 decreased, corresponding to the contraction of a lateral dimension of the cell. However, when strain was greater than 25–30%, the 002 *d*-spacings jumped back to nearly the original value and leveled off, as did the 010 *d*-spacings. Thus the crystal deformation is largely elastic to a strain of some 30%.

The behavior of the *d*-spacings could be explained by the internal rotation of the methylene group in the unit cell. By applying strain, it is likely that the *gauche* configuration of the methylene group rotated internally and the chain extended. This would be consistent with an increase of the 002 *d*-spacing and a decrease of the 010 spacings. However, when the strain was high enough to create localized plastic flow, the chains relaxed to their equilibrium state. Combining the relationship between strain

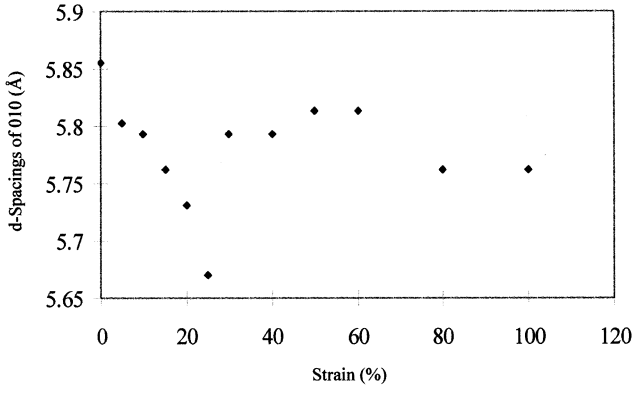

Fig. 8. The effect of strain on 010 *d*-spacing of fiber of processed draw ratio of 3.3:1 at 25°C.

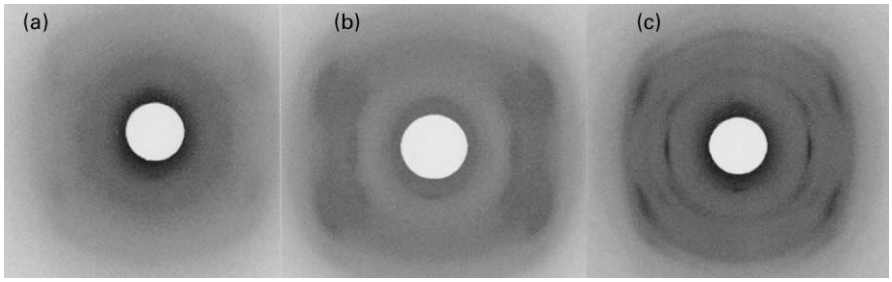

Fig. 9. Temperature effect illustrated by 2D WAXD pattern from fiber of processed draw ratio of 2:1, strain = 0: (a) $T =$ 25°C; (b) $T = 50$°C; (c) $T =$ 120°C.

and crystallinity shown in Fig. 6 with the cell dimension change in Fig. 7, it is clear that the increase in crystallinity corresponds to strain-induced crystallization and is accompanied by unit cell elongation, whereas plastic flow took place at strains above 30% and resulted in crystal destruction and the observed decrease in crystallinity with increasing strain.

4.1.3. The effect of temperature on crystallinity from WAXD

Shown in Fig. 9 are raster images of diffraction patterns of fibers of processed draw ratio 2:1 under 0% strain at 25, 50 and 120°C. It is observed that the crystallinity increases with increasing temperature. In Fig. 9(b) and (c), it was observed that the crystalline peaks are very broad, indicating very defective and/or small crystals. As mentioned above, this large degree of broadening prevented us from obtaining quantitative values of crystallinity for this series. Comparing Fig. 9(b) with (c), it is also noted that orientation decreases with increasing temperature. At this relatively high temperature, the crystallization effect is high and is not necessarily along the fiber axis. Detailed orientation analysis will be presented in a latter part of this paper.

4.1.4. The effect of strain at 120°C from both WAXD and SAXS

WAXD patterns at selected strains for fibers of processed draw ratio 2:1 at 120°C are shown in Fig. 10. By inspection, one sees that strains up to 40% might simply destroy crystals. The crystallinity dropped nearly to zero at 40% strain. This behavior was related to a high chain mobility at 120°C and a relaxation effect, which was greater than that at 25°C. Thus the effect of initial strain on crystallinity was opposite to that at 25°C.

Further application of strain to 50% began to induce crystallization, as seen in the WAXD pattern in Fig. 11(a). Fig. 11(b) shows the corresponding SAXS image, in which a weak two-lobe pattern is observed. This suggests a defective lamellar stacking. Applying the correlation function analysis described above, one obtains a long period of 7.7 nm. Thus intermediate strain about 50% begins to align chains and re-induce crystallization. Due to the relatively high mobility of and relatively high stress in the system, crystallites and amorphous regions begin to organize themselves into a stacked lamellar structure.

When strain was further increased to 120%, a pair of very weak and narrow streaks perpendicular to the meridian was observed near the third layer line on the WAXD pattern. These streaks are shown in Fig. 12, which has been processed so as to exaggerate the streak. The streaks imply a microfibrillar entity, perhaps the shish of a shish-kebab structure because the narrow streak is the reciprocal image of a long thin fibril. Since the corresponding SAXS pattern still showed a two-lobe pattern, which is similar to Fig. 11(b), this suggests that the lamellar to fibrillar transition has taken place. Such behavior has been observed in transmission electron microscope studies of plastic deformation in melt-crystallized polyolefins [16–18].

4.1.5. Orientation analysis

The orientation factor for the 010 reflection from fibers of draw ratio of 3.3:1 and 2:1 at 25 and 120°C was calculated

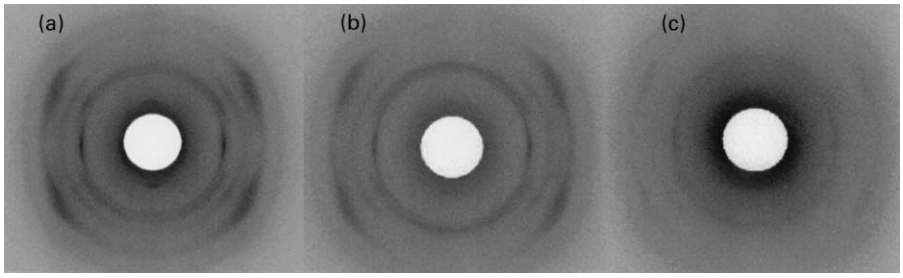

Fig. 10. Initial strain effect for fiber of processed draw ratio of 2:1 at 120°C: (a) strain = 0%; (b) strain = 15%; (c) strain = 40%.

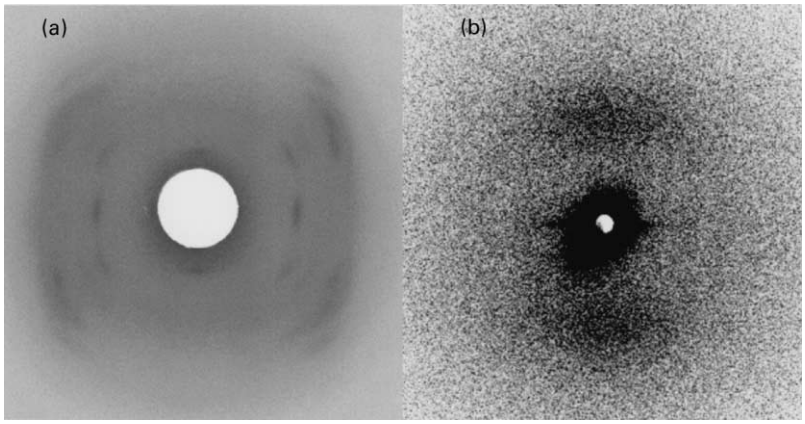

Fig. 11. Re-induced crystallization and defectively stacked lamellar formation at strain = 50% for fiber of draw ratio of 2:1 at 120°C: (a) raster image of WAXD pattern and (b) raster image of SAXS pattern.

as described above. The results are shown in Fig. 13. At 25°C for fibers of processed draw ratio of 2:1 and 3.3:1, the initial application of strain decreases the orientation factor. After a short plateau region, the orientation factor begins to drop again. The plateau and decay regions at intermediate or high strain correspond to the yielding phenomenon and the destruction of crystallites, respectively. The decrease of the orientation factor with the initial application of strain is intriguing. This decreasing orientation runs parallel to increasing crystallinity (compare Figs. 6 and 13 for fibers of processed draw ratio 3.3:1). This suggests that new, strain-induced crystals have lower orientation than those existing at the outset. It has been reported for several polymer systems that the mean orientation of crystallites grown in an extended melt is generally greater than that of the melt from which they form [19–23]. This behavior appears to be the result of the selection of the most highly oriented chains for nucleation events [19,23–25]. The remaining pool of uncrystallized chains therefore has a lower orientation than do the initial crystals. Crystals forming subsequently from this remnant should produce crystals of increasingly lower orientation as crystallization progresses [25–27]. This concept can qualitatively explain the observed decrease in crystal orientation with initial applied strain at room temperature. Furthermore, the matrix out of which the crystallization is induced is suspected to be the rigid amorphous phase or mesophase because strain cannot induce crystallization from initially undrawn fibers at room temperature, as stated in Section 4.2. The initial increase in orientation with applied strain at 120°C would appear to be further selected nucleation of highly oriented material, prior to depletion of the pool of sufficiently oriented material. The final sharp increase of orientation with strain at this temperature may represent the re-creation of molecular orientation conditions favoring the most oriented noncrystalline population.

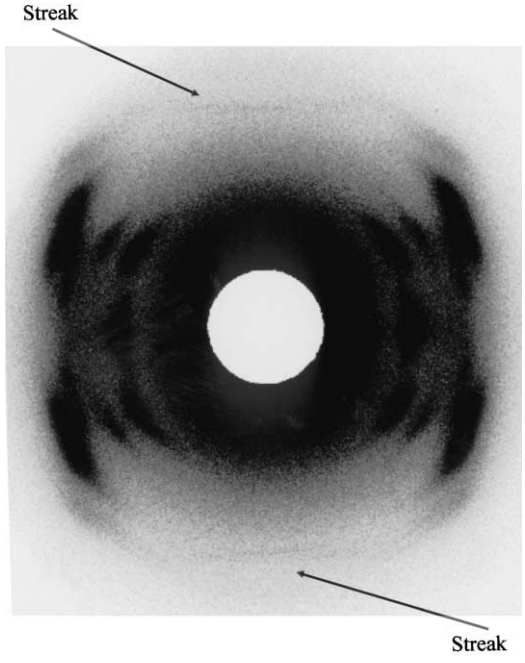

Fig. 12. Raster image for WAXD pattern from fiber of processed draw ratio of 2:1 at 120°C, strain = 120%, showing the streak perpendicular to the fiber axis.

4.2. As-spun fibers

4.2.1. Intermediate phase formation from WAXD pattern

At 25°C, the WAXD patterns for undrawn fibers at all strain levels consist only of amorphous halos (not shown). This suggests that strain alone cannot induce crystallization from the unoriented amorphous phase. At 50°C, two broad and weak equatorial arcs come into being, as shown in Fig. 14(a), suggesting that crystallization begins taking place. However, application of strain of only 5% destroys the defective crystals, as shown in Fig. 14(b), demonstrating the low stability of these crystallites.

Fig. 15 shows the effect of heating to 120°C and subsequent stretching on as-spun fibers. Fig. 15(a) is a WAXD pattern from an as-spun, unstretched fiber held at 120°C. After stretching to 60%, the pattern appears as in

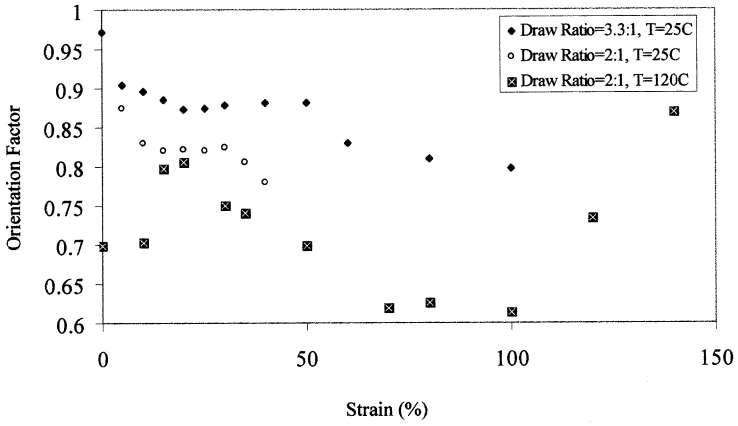

Fig. 13. Orientation factor versus strain curve.

Fig. 15(b), and after 300% as in Fig. 15(c). In the undrawn state, two new equatorial reflections appear, with *d*-spacings of 6.05 ± 0.07 and 4.76 ± 0.05 Å. These reflections can not be assigned to any known *d*-spacings. Comparing Fig. 15(a) and (b), it appears that strain acts to orient these newly formed crystals. Further application of strain transformed these new crystals to the equilibrium structure, as shown in Fig. 15(c).

4.2.2. Meridianal SAXS streaks

The effect of strain on the small angle signal is shown in Fig. 16. At zero strain, since only an amorphous halo is observed in the WAXD patterns, the equatorial streak in Fig. 16(a) likely originates from the existence of axially extended micro-voids, since strain-induced fibrillar crystals appear to require the existence of a drawing-induced oriented mesophase, and the conditions for such a precursor are not met in the as-spun fibers. Application of strain induces a meridianal streak, and also intensifies the equatorial streak, as shown in Fig. 16(b). Given that this streak is induced by strain, it is likely that it represents micro-crazing with the craze plane normal to the tensile (fiber) axis. In addition, the concentration of entities, i.e. elongated microvoids associated with the equatorial streak, is increased.

It is necessary to mention that in other situations (elevated temperature and application of strain), the shape of the SAXS pattern of the as-spun fibers was simply an equatorial streak.

5. Discussion

5.1. The effect of temperature and strain on crystallinity and orientation

The application of strain at room temperature (well below T_g) to spun and drawn, partially crystallized PTT fibers initially induces further crystallization. At the same time, the mean orientation of the entire crystallite population decreases. In this low strain region (<40% for material processed to a draw ratio of 2.0), elastic deformation of the existing crystals is observed. Larger applied strains lead to plastic deformation and to the destruction of crystallites. On the other hand, the initial application of

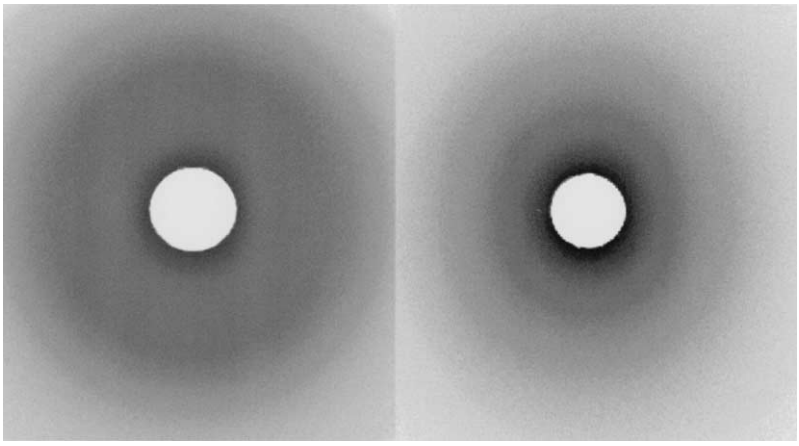

Fig. 14. 2D WAXD pattern illustrating strain effect on undrawn fibers at 50°C: (a) strain = 0%; (b) strain = 5%.

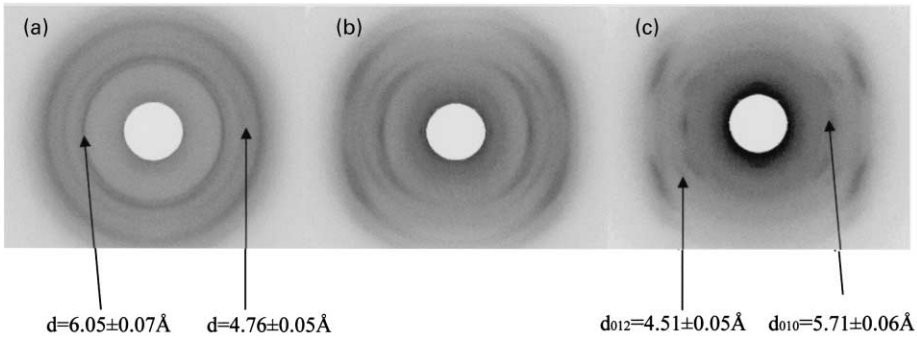

Fig. 15. 2D raster image of WAXD pattern illustrating the formation of new transitional phase in undrawn fibers at 120°C: (a) strain = 0%; (b) strain = 60%; (c) strain = 300%.

stress at 120°C, well above T_g, promotes immediate crystal destruction.

Below T_g, only localized translation or rotational motion is possible. Modest extensional stresses — below those necessary for plastic flow — are seen to promote crystallization in this system. This would seem to indicate that chain segments, which are parts of sequences which are already relatively well aligned and not far from crystalline registry can be forced, under such stress, to shift locally into crystalline registry. Because the motions are so localized, the crystallites formed at such sub-T_g temperatures must assume the orientation of the noncrystalline sequences from which they come. Given that prior crystallization under very high strain already had utilized the most highly aligned segments, sub-T_g strain-induced crystals can only lower the mean crystal orientation and this is what is observed. At a sufficiently high stress level, intracrystallite slip is induced and is observed macroscopically as yielding. At this stage, the applied strain is borne by such long-range flow and the intracrystalline and intra-amorphous stresses are decreased. No strain-induced crystallization would be expected under these low-stress conditions and the net effect would be crystal destruction, as observed.

The results of the stretching of as-spun fibers at 25°C also support this view. The applied strain did not induce crystallization from the poorly oriented amorphous phase. In these undrawn fibers, the chains were more nearly random coils and local motion at 25°C could not bring chain segments into substantial parallel alignment. The stress could only move the chain segments locally to create microcrazes.

For drawn fibers, the effect of increasing temperature under no applied strain is to increase the crystallinity and decrease the orientation, as seen in Fig. 9. At 120°C, the application of strain gradually destroys crystallites. This suggests once crystallites are destroyed at this temperature, relaxation kinetics are greater than crystallization kinetics and no crystallization is possible. At high strain, however, sufficient chain orientation is induced to promote crystallization kinetics over relaxation.

For as-spun fibers at zero strain, very defective crystals formed at 50°C. These poorly formed crystallites were destroyed by the initial application of strain. At 120°C, a transitional phase formed. The initial application of strain oriented this phase and further application of strain (300%) transformed this crystal to the equilibrium structure. No significant crystallinity decrease was observed, suggesting that crystallization kinetics were always higher than the relaxation kinetics in as-spun fibers at 120°C.

5.2. Morphology transformation in spun and subsequently drawn fibers at 120°C

For spun and drawn fibers of draw ratio of 3.3:1 at 25°C, WAXD patterns showed crystallinity, while SAXS patterns only have an equatorial streak. The streaks may originate from microfibrillar entities coexisting with intervening amorphous materials. At 120°C, upon

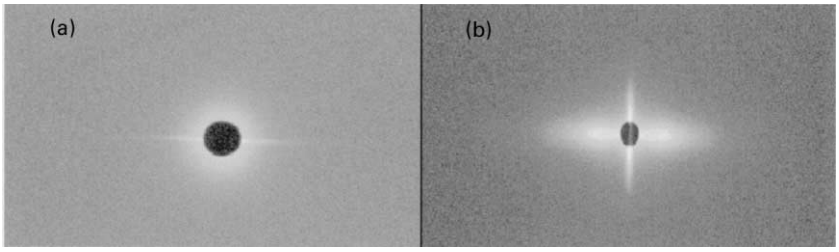

Fig. 16. Raster image of SAXS pattern from undrawn fibers at 25°C: (a) strain = 0%; (b) strain = 150%.

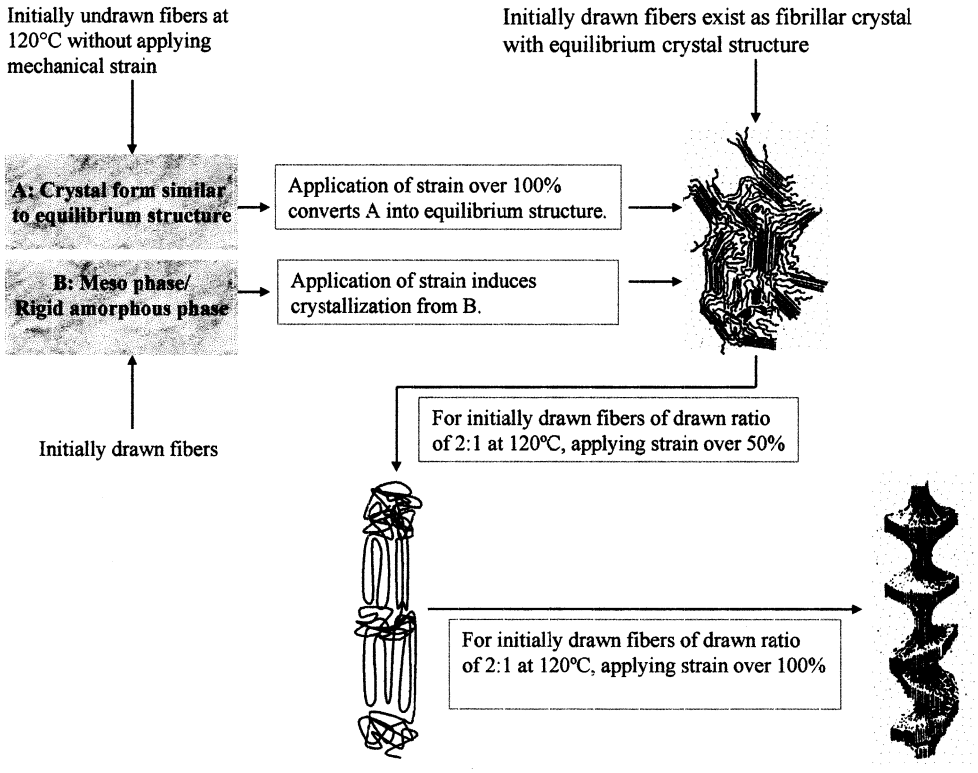

Fig. 17. Diagram summarizing phase and morphology transformation of PTT fibers.

application of strain on already heat-drawn fiber, the morphology undergoes a series of changes. Initial application of strain creates localized plastic flow and destroys crystallites. During further application of strain to about 50%, the system begins to reorganize into a defectively stacked lamellar structure. Further application of strain above 100% allows chains to extend, promotes chain extension, as suggested by the streak shown in Fig. 12, and induces the formation of narrow extended chain crystals. A mixture of defectively stacked lamellae and thin fibrillar crystals describes the morphology at this stage.

The morphology transformation in as-spun and in spun and drawn fibers as well as that in initially undrawn fibers under applied strain and temperature is sketched in Fig. 17.

6. Conclusions

The temperature and strain effects on as-spun and on spun and subsequently drawn PTT fibers were examined:

1. *For spun and subsequently drawn fiber*:
   (a) At room temperature, strain first induces crystallization and then gradually destroys the crystals. The decreasing orientation of the crystals induced by the initial strain suggests that a rigid amorphous phase or mesophase exists in the previously drawn fibers.
   (b) At room temperature, the cell dimension changes with the increasing strain, possibly due to internal rotation of the methylene group in the unit cell.
   (c) With increasing temperature, crystallinity increases and orientation decreases in the previously drawn fibers.
   (d) Only at 120°C and strain greater than 50% can the formation of defectively stacked lamella structure be induced. The SAXS patterns of other cases for the previously drawn fibers are featured by an equatorial streak.
   (e) At 120°C and strain over 100%, narrow streaks perpendicular to meridian, which suggests the existence of narrow extended chain crystals, i.e. the shish of a shish-kebab structure.
2. *For previously undrawn fiber*:
   (a) Stretching at 25°C cannot induce crystallization.
   (b) At 50°C, very defective crystals form at zero strain, which are destroyed by application of strain. This suggests that the effect of relaxation of the chain is much greater than the crystallization effect.
   (c) At 120°C, a transitional phase other than the equilibrium structure forms. Initial application of strain orients these crystals and further application of strain (300%) transforms this crystal to the equilibrium structure. No significant crystallinity decrease is observed, suggesting that the crystallization rate is higher than the relaxation rate.
   (d) At 25°C, application of strain induces a meridianal

streak in the SAXS pattern, suggesting induction of microcrazes with the craze plane normal to the fiber axis.

Acknowledgements

This work was supported by NSF GOALI grant DMR-9629825.

References

[1] Desborough IJ, Hall IH, Neisser JZ. Polymer 1979;20:545.
[2] Dandurand SP, Perez S, Revol JF, Brisse F. Polymer 1979;20:419.
[3] Jakeways R, Ward IM, Wilding MA, Hall IH. J Polym Sci: Polym Phys Ed 1975;13:799.
[4] Ward IM, Wilding MA, Brody H. J Polym Sci: Polym Phys Ed 1976;14:263.
[5] Marquardt DW. J Soc Ind Appl Math 1963;11:431.
[6] BaltaCalleja FJ, Vonk CG. X-ray scattering of synthetic polymers. Amsterdam: Elsevier, 1989.
[7] Hermans PH, Platzek P. Kolloid Z 1939;88:68.
[8] Hermans PH, DeBooys JJ. Kolloid Z 1939;88:73.
[9] Hermans PH, Hermans JJ, Vermaas D, Weidinger AJ. J Polym Sci 1947;3:1.
[10] Alexander LE. X-ray diffraction methods in polymer science. New York: Wiley, 1969.
[11] Wilchinsky ZW. J Appl Phys 1960;31:1969.
[12] Stein RS. J Polym Sci 1958;31:327.
[13] Strobl GR, Schneider M. J Polym Sci: Part B: Polym Phys 1980;18:1343.
[14] Ruland W, Dewaelheyns A. J Sci Instrum 1967;44(3):236.
[15] Hsiao BS, Kennedy AD, Leach RA, Chu B, Harney P. J Appl Cryst 1997;30:1084.
[16] Sakaoku K, Peterlin A. Makromol Chem 1967;108:234.
[17] Miles M, Petermann J, Gleiter H. J Macromol Sci 1976;B12:523.
[18] Gohil RM, Petermann J. J Polym Sci: Polym Phys Ed 1979;17:525.
[19] Krigbaum WR, Roe R-J. J Polym Sci 1964;2A:4391.
[20] Dismore PF, Statton WO. J Polym Sci 1966;13C:133.
[21] Dumbleton JH, Polym J. J Polym Sci 1969;7A-2:667.
[22] Dumbleton JH. Polymer 1969;10:539.
[23] Krigbaum WR, Tag T. J Polym Sci: Polym Phys Ed 1979;17:393.
[24] Ziabicki A, Jarecki L. Colloid Polym Sci 1978;256:332.
[25] Abhiraman AS. J Polym Sci: Polym Phys Ed 1983;21:583.
[26] Desai P, Abhiraman AS. J Polym Sci: Polym Phys Ed 1985;23:653.
[27] Yoon KJ, Desai P, Abhiraman AS. J Polym Sci: Polym Phys Ed 1986;24:1665.